He discharges with transition on GOLEM Spectroscopic Study

B. García[1]†, M. Kato[2]‡ V. Weinzettl[3] and D. Naydenkova[3]

[1]Aix-Marseille University, 58 boulevard Charles-Livon, 13007 Marseille, France
[2]FNSPE, Czech Technical University in Prague, Břehová 7, 115 19 Prague 1., Czech Republic
[3]Institute of Plasma Physics of the Czech Academy of Sciences, U Slovanky 2525/1a, 182 00 Prague 8, Czech Republic

1. Introduction

The spontaneous formation of a transport barrier without the use of externally forced edge plasma polarization was first observed in 2018 in helium discharges with a limiter plasma configuration on the GOLEM tokamak by Macha [1]. This phenomenon is commonly observed in divertor plasma configurations as exemplified in [1], rather than in circular plasmas such as those in GOLEM.

These regimes were re-investigated during the SUMTRAIC 2024 event, see https://indico.ipp.cas.cz/event/25/, where it was found that the transport barrier was clearly formed at high plasma currents (about 2 kA). This formation was accompanied by a color transition from orange to blue, correlated with intense impurity line emissions. Several low-Z impurity spectral lines were identified and it was ruled out that the effect could be related to the position of the Langmuir probe in the plasma. However, it remained unclear whether specific plasma parameters, such as plasma current, magnetic field, or gas puff, define the threshold for barrier formation or how the color transition relates to the time-dependent behavior of impurity emissions.

The primary goal of two tasks of the EMTRAIC 2024, probe (Group 1) and spectroscopic (Group 2) measurements on GOLEM, event was to further investigate the existence of transport barriers under these conditions, identify the critical plasma parameters required for their formation, and explore the relationship between barrier formation and breakdown conditions. Additionally, the study aimed to analyze the measured spectral data to better understand the role of impurity emissions in this process. The report is structured as follows. Section 2 introduces the experimental set-up, which is used for the measurements overviewed in Section 3. Section 4 then concludes the reached results.

2. Experimental Setup

2.1. *GOLEM Tokamak*

New experiments were conducted on the GOLEM tokamak (Figure 1), currently located at the Czech Technical University in Prague. It features a circular plasma cross-section, defined by the molybdenum limiter, a typical plasma current of up to 5 kA, a toroidal magnetic field of less than 0.5 T with a sinusoidal waveform, a line-averaged density of up to $\sim 3\times10^{19}\mathrm{m}^{-3}$, and a core electron temperature below 100 eV in hydrogen discharges (about a half value is estimated for He plasmas). The working gases include

† Email address for correspondence: beatriz.garcia@etu.univ-amu.fr
‡ Email address for correspondence: katomomo@fjfi.cvut.cz

hydrogen (H), deuterium (D), helium (He), and argon (Ar); however, only He discharges with transport barrier formation were investigated in this study.

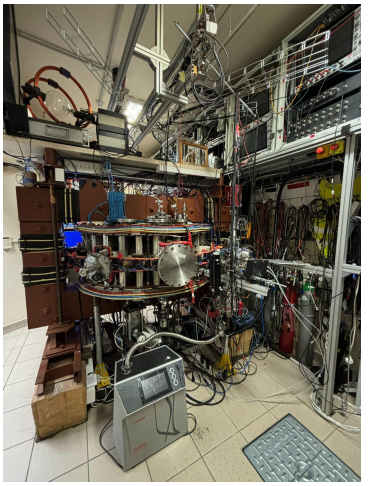

Figure 1: GOLEM tokamak.

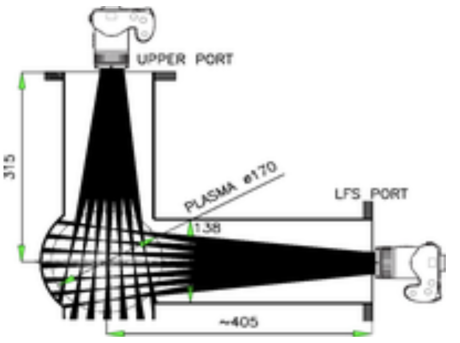

Figure 2: High-speed cameras configuration.

2.2. *Diagnostics and Instrumentation*

The diagnostics and plasma parameters included plasma current (I_p), loop voltage (U_{loop}), and toroidal magnetic field (B_t), all measured using magnetic diagnostics; two high-speed color cameras; and five compact spectrometers covering the near-ultraviolet, visible light, and near-infrared spectral regions.

2.3. *Cameras and Spectrometers*

The arrangement of the two high-speed cameras is shown in Figure 2. One camera provided a top view with radial resolution, while the other offered a radial view with vertical resolution.

The five compact Czerny–Turner type spectrometers observe the poloidal plasma cross-section through the lower vertical diagnostic port, with all optical fibers sharing a common vacuum feedthrough and collection lens to ensure the same field of view. Among them, the IRVISUV spectrometer, which has the broadest spectral range (185–1110 nm) and a resolution of approximately 0.45 nm/px, and the H-alpha spectrometer (630–680 nm, 0.025 nm/px) were primarily used in this study. The remaining spectrometers include UV (248–472 nm, 0.11 nm/px), VIS (460–663 nm, 0.10 nm/px), and IR (654–1084 nm, 0.21 nm/px). Details of the spectral calibration for the H-alpha and UV spectrometers are provided in the appendix.

3. Results and discussion

3.1. I_p *scan*

A plasma current scan was conducted to determine the critical values for transport barrier formation. The set of 11 discharges performed on the tokamak, each with different current drive voltages (U_{CD}), resulting in varying maximum plasma currents, is summarized in the appendix (Table 1). For completeness, the discharge with the highest $U_{CD} = 800$V (#47111) was included, as it was carried out under the same conditions

by the probe group as part of a separate task in EMTRAIC 2024. All other discharge parameters were kept the same during the scan.

Figure 3 illustrates the time evolution of basic plasma parameters for discharges with maximum, minimum, and intermediate current drive voltages. The data show that increasing U_{CD}, and consequently I_p, causes a delay in breakdown and results in shorter discharge durations. Additionally, this shift in the discharge timing relative to B_T slightly reduces the magnetic field as U_{CD} increases.

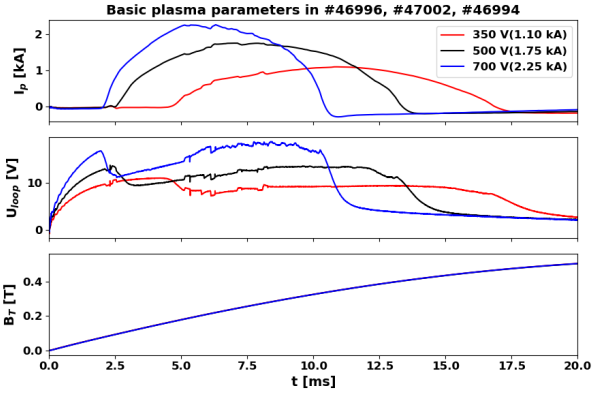

Figure 3: Time evolution of basic plasma parameters during He discharges with transport barrier formation.

The fast camera images of the color transition for the same three discharges are presented in Figure 4 (left), with the corresponding RGB components(right). The discharge with the highest I_p exhibits the most intense color transition, occurring earliest in the discharge. Before the transition, the red RGB component is saturated, while the green component remains relatively high compared to the blue, resulting in the observed orange color during the transition. Following the transition, the red component decreases, and the blue component increases. This RGB behavior is consistent across all discharges. However, as I_p decreases in the scan, the color transition becomes weaker. In the case of the lowest I_p, the transition occurs the latest in discharge and is the longest in duration.

The IRVISUV spectrometer spectra were analyzed for 2 ms exposures before and after the color transition in the selected discharges, identifying 59 spectral lines. Figure 5 (left) shows the measured spectra before the transition in the yellow to red range, dominated by strong He I lines. The spectra after the transition are shown in Figure 5 (right) in the blue to green range, where there is the highest increase of lines intensities, with peaks from H I, N II, C II, Cl II, O I, O II, and possibly C III. However, C III identification could not be confirmed due to overlapping with N II and O II spectral peaks. Most of these lines were confirmed also before the transition at weaker intensities. Unidentified lines were attributed to low signal-to-noise ratio (S/N).

The time evolution of well defined spectral peaks of working gas and some plasma impurities was analyzed to examine their relationship to the color transition (Figures 6, 13 and 8). Additionally, each line was studied across I_p values ranging from 1.10 to 2.80 kA. The intensity of all spectral lines increases with I_p, consistent with the relationship $I \sim n_e \times n_{ion,lower\ transition\ state} \times C_{exitation}(n_e, T_e)$, with electron and ion densities, where the last term is the rate coefficient, which strongly depends on electron temperature, thus coupled with Ip, because ohmic heating is the only heating method

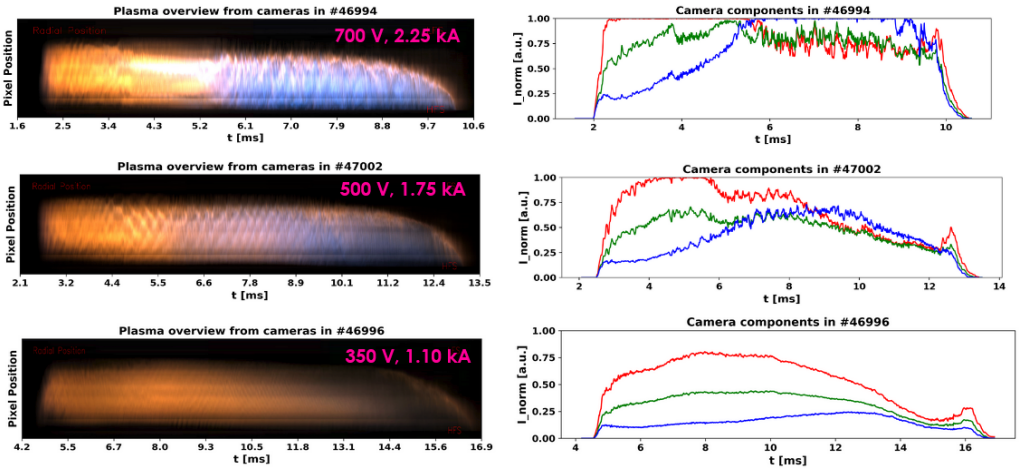

Figure 4: Images from the fast cameras showing the color transition at different I_p values (left) and the corresponding RGB components (right).

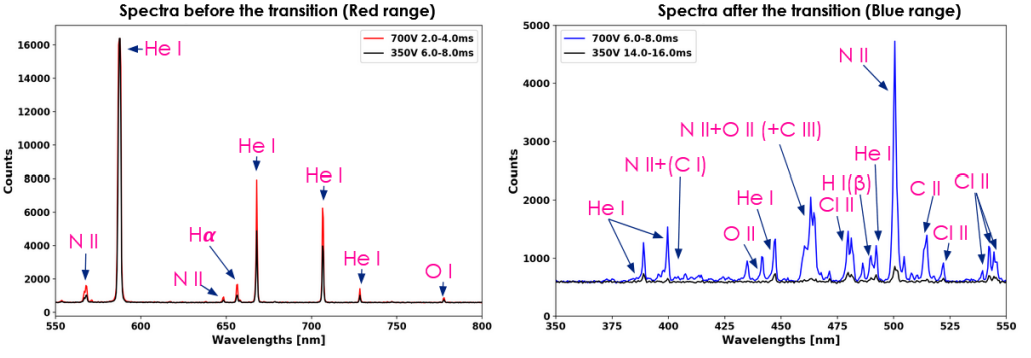

Figure 5: Spectra before and after the color transition

of the GOLEM plasmas. This intensity trend aligns with probe measurements showing higher T_e at increased I_p. Most importantly, no critical I_p value was identified for the presence of these peaks. There is also no deviation from a smooth behaviour of the observed lines with Ip and the color transition seems to be an effect also smooth in time, although it is much faster for Ip higher than 2 kA. Unfortunately, our spectroscopic observations were limited by the time resolution of 2 ms, given by the used detector.

In the next paragraphs, an example of the typical spectral line behavior for helium (working gas) and impurities (H, C) will be provided. It should be mentioned that the lines of the same ionization state and of the same element have usually a very similar behavior (also proved by our measurements), therefore, there is no important information hidden in other observed lines. Figure 6 shows the He I 667.8 nm line (working gas). Its intensity decreases after reaching its maximum early in the discharge, but a connection to the color transition could not be confirmed due to the 2 ms time resolution of the spectrometer.

The H_α 656.3 nm line (Figure 13) is a common impurity with sources including atmospheric water vapor (H_2O), plastics in cabling or other in-vessel materials, or prior discharges using hydrogen as the working gas. At high I_p its behavior resembles the He

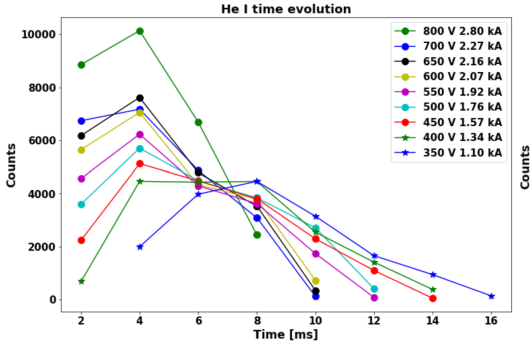

Figure 6: He I (667.8 nm) time evolution

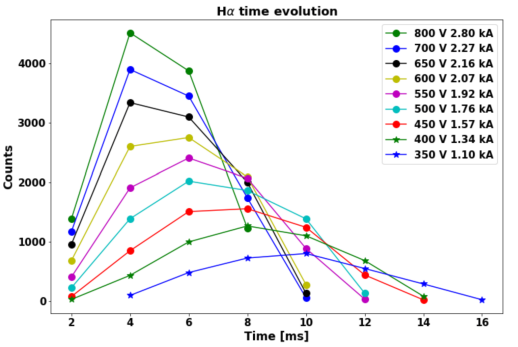

Figure 7: H_α (656.3 nm) time evolution

lines due to the spectrometer's limited 2 ms resolution. However, at lower I_p, the intensity of the line reaches its maximum later, and its decay is noticeably slower.

The C II 657.8 nm line (Figure 8) exhibits a similar dependence to the previous H_α line but takes even longer to reach its maximum intensity. The deviation observed in the 2.80 kA line is attributed to the fact that this shot was conducted on a different day, indicating a slightly modified plasma contamination by carbon.

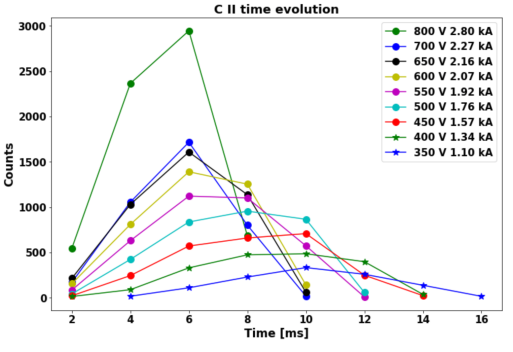

Figure 8: C II (657.80nm) time evolution

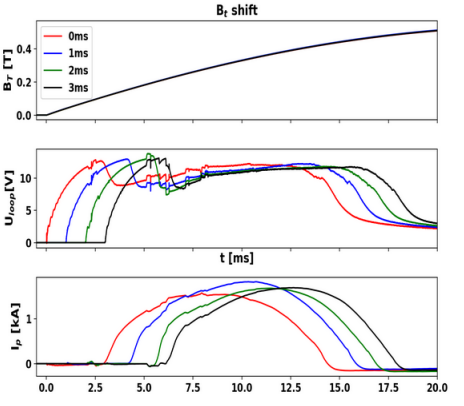

Figure 9: Time evolution of basic plasma parameters during the B_t shift scan.

3.2. *B_t shift scan*

We conducted additional experiments with a shifted toroidal magnetic field to investigate its amplitude's influence and the breakdown conditions on the transition. Four shots were performed (see appendix, Table 2), varying the time delay (0–4 ms) for the capacitors to start charging the current drive, thereby shifting the discharge's B_t (increasing with the delay) and breakdown (Figure 9). The U_{CD} was kept constant for all discharges, resulting in similar I_p values.

The fast camera images from these discharges are shown in Figure 10 (left), along with their corresponding RGB components (right). The time axis for the figure has been adjusted to align the color transitions, which are very similar across all discharges. This is confirmed by the RGB components (small differences can be attributed to minor changes in I_p over the scan). Since the significant time shift of the breakdown, and therefore

the magnitude of B_t, had no observable effect on the behavior or timing of the color transition, it can be concluded that the breakdown conditions do not play a primary role in the transition itself. However, the MHD activity, indicated by fluctuations of the RGB components, is notably affected, being strongly suppressed at higher time delays corresponding to increased B_t values.

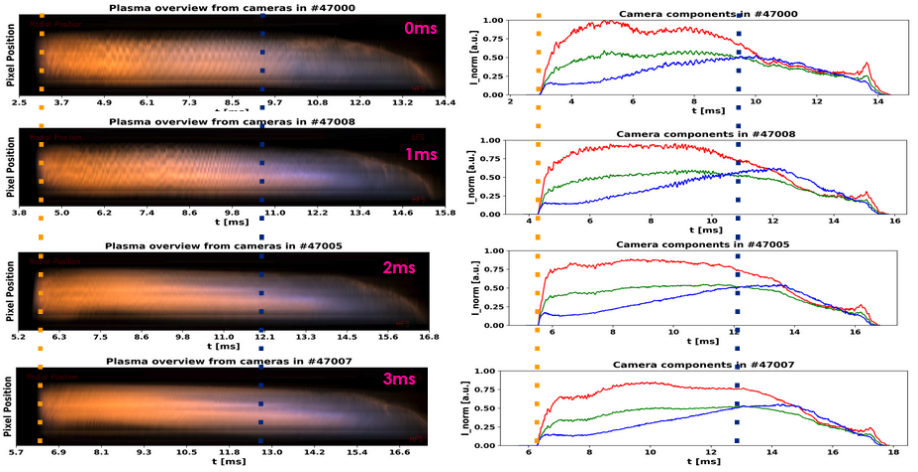

Figure 10: Images from the fast cameras showing the color transition for different B_t shifts (left) and the corresponding RGB components (right).

3.3. *Challenges in Identifying High Ionization States in Spectra*

Although spectral lines of the higher ionization states of the present elements were anticipated, particularly at higher I_p or after transport barrier formation, none have been clearly identified across all observed elements. Apart from the C III triplet near 465 nm (possible overlapping with other impurity lines), no evidence of such lines, e.g. He II, was found. Given the probe-measured electron temperature near the separatrix ($\sim$10 eV) and Spitzer conductivity estimates of $\sim$40 eV in the core, it is unlikely the plasma was too cold. The most probable explanation is that the spectrometers' sensitivity was insufficient, with these lines hidden by noise which is likely amplified by neutral gas inflow from microleaks in the vacuum vessel. Note that excitation rates are very different over different lines of the ionization states of the involved impurities. Therefore, some of them can be easily hidden in the noise or overlapped with stronger lines.

4. Conclusions

The edge plasma barrier formation in the GOLEM tokamak with helium discharges, observed through the plasma color transition by fast cameras, was linked to an increase in impurity radiation measured by compact spectrometers, which became dominant after the barrier forms. The color change from orange to blue and intensity were more pronounced at higher I_p, occurring earlier and faster in the discharge. No critical I_p threshold for barrier formation was identified, although the transition was weaker and occurred later at $I_p \approx 1$ kA. While the influence of B_t on the discharges was isolated and not associated with barrier formation, it significantly affected MHD activity, with stronger B_t correlating to reduced MHD activity. More detailed analysis with the emission modeling will be the further work.

5. Acknowledgements

This experimental work took place at the IPP, Prague with in the EMTRAIC event. The authors would like to thank Dr.Jordan for entire organization of the event and dedicated support.

References

[1] P. Macha, J. Adamek, J. Seidl, J. Stockel, V. Svoboda, G. Van Oost, L. Lobko, and J. Krbec, *Spontaneous formation of a transport barrier in helium plasma in a tokamak with circular configuration*, International Atomic Energy Agency Nuclear Fusion, 2023

6. Appendix

6.1. *Shots Tables*

#Shot	U_{CD} [V]	$I_{p,max}$[kA]
46993	350	1.10
46996	350	1.10
46998	400	1.35
47000	450	1.55
47002	500	1.75
47001	550	1.90
46999	600	2.05
46997	650	2.15
46991	700	2.20
46994	700	2.25
47111	800	2.80

Table 1: I_p scan shots

#Shot	t_{shift} [ms]	U_{CD} [V]	$I_{p,max}$ [kA]	B_t (at $I_{p,max}$) [T]
47000	0	450	1.6	0.27
47008	1	450	1.8	0.35
47005	2	450	1.7	0.37
47007	3	450	1.7	0.39

Table 2: B_t scan shots

6.2. *Spectral Calibration*

The spectral calibration was performed by replacing the tokamak plasma source with a spectral calibration lamp emitting known spectral lines. The optical fiber connected to the detector was redirected to the calibration source. The positions of the measured spectral lines were then assigned to their tabulated wavelengths and fitted with a cubic polynomial for wavelength calibration.

6.2.1. *Halpha Spectrometer*

A Ne source was used to calibrate the H-alpha spectrometer, where the measured spectrum is shown in Figure 11. The wavelength calibration for the H-alpha spectrometer is given by the following polynomial fit:

$$\lambda[nm] = 629.78 + 0.03x - 4.00 \cdot 10^{-6}x^2 + 7.20 \cdot 10^{-11}x^3$$

Where x is the pixel number. Figure 13 compares the calibration fit with the manufacturer-provided spectral axis, including the spectral lines used for calibration. The difference between the measured wavelength and the manufacturer's calibration was approximately $\Delta\lambda$ ~0.1 nm. The spectral resolution per pixel was determined to be ~0.025 nm/pixel (slightly changing with wavelength), corresponding to a systematic shift of approximately 4 pixels which is therefore non-negligible and the new spectral calibration should be used for the spectral measurements with the Halpha spectrometer. The full-width at half-maximum (FWHM) was measured as 0.055 nm and can be interpreted as the intrumental line broadening, since the broadening of the emitted lines caused by the calibration source itself is negligible (cold source).

6.2.2. *UV Spectrometer*

A Hg source was used to calibrate the UV spectrometer, where the measured spectrum is shown in Figure 12. The wavelength calibration for the H-alpha spectrometer is given by the following polynomial fit:

$$\lambda[nm] = 246.87 + 0.12x - 3.85 \cdot 10^{-6}x^2 + 8.24 \cdot 10^{-11}x^3$$

Figure 14 compares the calibration fit with the manufacturer-provided spectral axis, including the spectral lines used for calibration. The wavelength difference relative to the manufacturer's calibration was approximately $\Delta\lambda$ ~0.07 nm near the center of the spectra range (~ 350 nm) and $\Delta\lambda$ ~0.09 nm in the blue region (~ 450 nm), indicating a small variation. The spectral resolution per pixel was ~0.011 nm/pixel near the center and ~0.106 nm/pixel in the blue region, therefore, the difference between the calibration in the region of interest (380-450 nm) can be neglected.

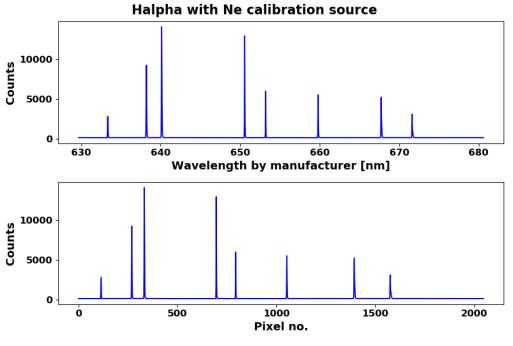

Figure 11: Measured spectrum of the Ne source for the H-alpha calibration.

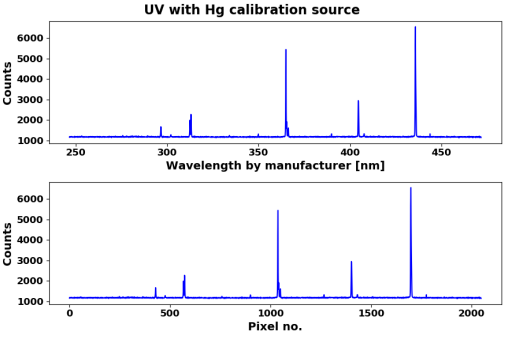

Figure 12: Measured spectrum of the Hg source for the UV calibration.

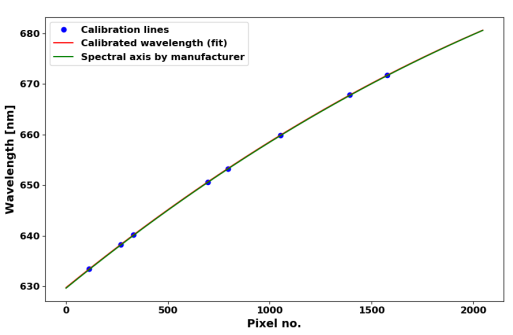

Figure 13: H-alpha calibration fit compared to the spectral axis provided by the manufacturer.

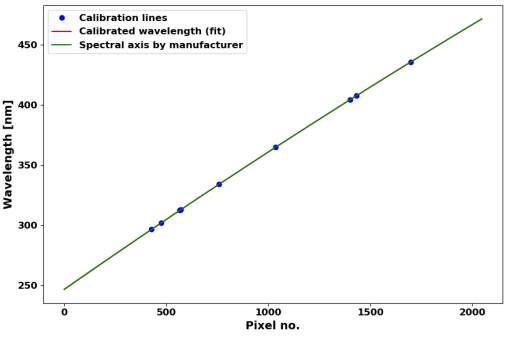

Figure 14: UV calibration fit compared to the spectral axis provided by the manufacturer.